Scientia Iranica, Vol. 6, No. 2, pp 122–130

SCIENTIA
IRANICA

Computation of High Reynolds Number, Parabolized Navier-Stokes Equations Based on Upwind Algorithm

H. Emdad*, M.M. Alishahi[1] and E. Goshtasbi Rad[1]

A three-dimensional Parabolized Navier-Stokes (PNS) code has been developed for calculating supersonic turbulent flow. The code employs an upwind algorithm throughout the subsonic and supersonic zones. The algorithm is implicit and uses a cell centered finite volume scheme. To validate the code, turbulent supersonic flow around Secant Ogive Cylinder (SOC) and Tangent Ogive Cylinder (TOC) is computed and compared with experimental measured data. Results are acceptable up to 6° angle of attack. By increasing the angle of attack to 10°, the separation zone becomes dominant and the pressure distribution would have an error up to 20% of the experimental data.

INTRODUCTION

PNS equations have been used successfully in computing complex steady supersonic viscous flow fields. A nonlinear, implicit, space marching, finite difference algorithm based on the viscous subsonic layer method has been proposed by Schiff and Steger [1]. This method has been used by Sturek et al. [2,3] to compute the flow field about spinning and non-spinning secant ogive cylinder with and without boat tail. Sturek also has used Baldwin-Lomax turbulence model with and without modification. It concluded that the computed pressure distribution is in good agreement with the experiment up to 6° angle of attack.

Another scheme has been proposed by Vigneron et al. [4] using pressure splitting flux tensor for simplifying the decoding of the fluid dynamic variables from the marching direction flux vector. This scheme is based on a class of Alternating Direction Implicit (ADI) schemes developed by Beam and Warming [5], which solve time dependent equations such as unsteady Navier-Stokes equations. A new application based on the MacCormack explicit two step finite volume predictor corrector has been employed by Deese et al. [6]. One of the major drawbacks of the previous schemes is that central differencing of fluxes across flow field discontinuities tends to introduce errors into the solution in the form of local flow property oscillations. To control these oscillations, some types of artificial dissipation are required. The user must specify the correct smoothing parameter magnitudes through a trial and error process.

Another new application of the upwind algorithm in three-dimensional PNS equations has been proposed by Lawrence et al. [7-10]. This algorithm is implicit, using finite volume, and is validated through application to laminar hypersonic flows. In their study, the spatial propagation of flow field information is locally modeled using a steady version of Roe approximation of Riemann problem. In addition, the upwind algorithm is applied only outside the sonic line of the flow field and the subsonic region of the boundary layer is treated with a central differencing approach. This approach is taken because, in two dimensions, a degradation in stability was encountered when applying upwinding in a subsonic zone [8]. This work is an extension of the Lawrence scheme to turbulent flow field at supersonic speeds and implimentation of upwinding in a subsonic zone. The turbulence model developed by Baldwin-Lomax [11] and modified by Degani and Schiff [3] is employed. The resulting computer code has been validated by computing turbulent supersonic flow about two flying bodies, SOC and TOC. The flow about these models has been calculated at different angles of attack up

*. *Corresponding Author, Department of Mechanical Engineering, University of Shiraz, Shiraz, I.R. Iran.*
1. *Department of Mechanical Engineering, University of Shiraz, Shiraz, I.R. Iran.*

to 10° and are compared with experimental data [12].

GOVERNING EQUATIONS

The motion of a fluid is governed by conservation laws of mass, momentum and energy. The non-dimensional form of Navier-Stokes equations is,

$$\frac{\partial \underline{U}}{\partial t} + \Delta(\bar{\bar{H}}) = 0 \ , \tag{1}$$

where,

$$\bar{\bar{H}} = \bar{\bar{H}}_i - \bar{\bar{H}}_v \ . \tag{2}$$

$\underline{U}$ is the vector of the conservative variables (i.e., density, momentum and total energy) and is expressed as:

$$\underline{U} = \{\rho, \rho\underline{u}, E_t\}^T \ . \tag{3}$$

$\bar{\bar{H}}_i$ and $\bar{\bar{H}}_v$ represent the inviscid and viscous flux tensor, respectively, and are defined as:

$$\bar{\bar{H}}_i = \{\rho\underline{u}, \rho\underline{u}\underline{u} + P\bar{\bar{I}}, (E_t + P)\underline{u}\}^T \ , \tag{4}$$

$$\bar{\bar{H}}_v = \{0, -\tau, -\tau.\underline{u} + q\}^T \ , \tag{5}$$

where ρ is the density, P the pressure, $\bar{\bar{I}}$ the identity tensor, E_t the total energy and $\underline{u}$ the velocity vector given by:

$$\underline{u} = u\underline{i} + v\underline{j} + w\underline{k} \ . \tag{6}$$

Pressure and temperature are related to the conservative variables by the equation of state for a perfect gas:

$$P = \rho T, \tag{7}$$

$$P = (\gamma - 1)\left[E_t - \frac{\rho}{2}|\underline{u}|^2\right] \ , \tag{8}$$

with γ being the ratio of the constant specific heats. The stress tensor is given by Newton law:

$$\bar{\bar{\tau}} = \mu[\text{grad } \underline{u} + (\text{grad } \underline{u})^T] + \lambda \text{div } (\underline{u})\bar{\bar{I}} \ . \tag{9}$$

These viscosity coefficients are related by Stokes hypothesis also for a polyatomic gas:

$$\lambda = -\frac{2}{3}\mu \ . \tag{10}$$

The viscosity coefficient is obtained from Sutherland formula:

$$\frac{\tilde{\mu}}{\tilde{\mu}_\infty} = T^{\frac{2}{3}}\left(\frac{1+S}{T+S}\right) \ , \tag{11}$$

where $S = \tilde{S}/\tilde{T}_\infty$ with Sutherland constant in air being $\tilde{S} = 110.4K$.

The q in Equation 5 is obtained through Fourier law for the heat flux:

$$q = -K \text{ grad } T \ . \tag{12}$$

Also, the following relation between the dimensional heat conduction coefficient and viscosity coefficient is used:

$$\frac{\tilde{K}}{\tilde{K}_\infty} = \frac{\tilde{\mu}}{\tilde{\mu}_\infty} \ . \tag{13}$$

In three-dimensional Cartesian coordinates, the spatial coordinates are denoted by x, y and z and their corresponding velocity components by u, v and w. The equations have been non-dimensionalized (dimensional quantities are denoted by tilde and free stream values are denoted by ∞) in the following manner:

$$x, y, z = \frac{\tilde{x}, \tilde{y}, \tilde{z}}{\tilde{L}}, \quad u, v, w = \frac{\tilde{u}, \tilde{v}, \tilde{w}}{\sqrt{\tilde{P}_\infty/\tilde{\rho}_\infty}},$$

$$\rho = \tilde{\rho}/\tilde{\rho}_\infty, \quad P = \tilde{P}/\tilde{P}_\infty, \quad T = \tilde{T}/\tilde{T}_\infty, \quad E_t = \tilde{E}_t/\tilde{P}_\infty \ . \tag{14}$$

The dimensional free stream speed of sound ($\tilde{C}_\infty$) and free stream Mach (M_∞), Reynolds (Re_∞) and Prandtl numbers (Pr) are defined by the following reference quantities:

$$\tilde{C}_\infty = \sqrt{\gamma\tilde{P}_\infty/\tilde{\rho}_\infty}, \quad M_\infty = \frac{|\tilde{V}_\infty|}{\tilde{C}_\infty},$$

$$Re_\infty = \frac{\tilde{\rho}_\infty|\tilde{V}_\infty|\tilde{L}}{\tilde{\mu}_\infty}, \quad Pr = \frac{\tilde{\mu}_\infty\tilde{C}_P}{\tilde{K}_\infty} \ . \tag{15}$$

$\tilde{C}_P$ is the dimensional specific heat at constant pressure, $\tilde{V}_\infty$ the free stream velocity and Prandtl number, Pr, is assumed to be constant and equal to 0.72.

For a parabolized approximation, it is assumed that the Navier-Stokes equations are steady, the velocity outside of boundary layer is supersonic, the streamwise velocity component is everywhere greater than zero and the pressure gradient in the streamwise momentum equation is either omitted or treated with some other technique suitable to avoid a departure solution.

The scheme, which is developed by Vigneron et al. [4], is used in this study. This approach involves separating the streamwise flux vector (E) into two parts:

$$E = E^* + E^P \ , \tag{16}$$

where,

$$E = \{\rho u, \rho u^2 + P, \rho uv, \rho uw, (E_t + P)u\}^T,$$

$$E^* = \{\rho u, \rho u^2 + \omega P, \rho uv, \rho uw, (E_t + P)u\}^T,$$

$$E^P = \{0, (1-\omega)P, 0, 0, 0\}^T. \quad (17)$$

Based on this marching scheme, PNS equations are parabolic-hyperbolic and are stable in the subsonic region, if:

$$\omega = \min . \left[1, \frac{\sigma\gamma M_\xi^2}{1 + (\gamma - 1)M_\xi^2}\right] , \quad (18)$$

where M_ξ is the streamwise Mach number and σ the safety factor equal to 0.8. The gradient of E^P is usually neglected so that the steady form of Equation 1 becomes hyperbolic-parabolic in nature [13,14].

TURBULENCE MODEL

The two layer Baldwin-Lomax turbulent model [11] has been used successfully throughout many applications of PNS and thin layer Navier-Stokes equations. For the inner layer, μ_t, the eddy viscosity coefficient is defined by:

$$(\mu_t)_{\text{inner}} = \rho l^2 |\Omega| , \quad (19)$$

where l is the mixing length equal to:

$$l = ky[1 - \exp(-y^+/A^+)] , \quad (20)$$

where k and A^+ are constant and equal to 0.41 and 26, respectively, $|\Omega|$ is the magnitude of the local vorticity vector and is defined as:

$$|\Omega| = \sqrt{\left(\frac{\partial u}{\partial y} - \frac{\partial v}{\partial x}\right)^2 + \left(\frac{\partial v}{\partial z} - \frac{\partial w}{\partial y}\right)^2 + \left(\frac{\partial w}{\partial x} - \frac{\partial u}{\partial z}\right)^2} , \quad (21)$$

and:

$$y^+ = \frac{\sqrt{\rho_w \tau_w}}{\mu_w} y , \quad (22)$$

where, ρ_w, τ_w and μ_w are density, shear stress and viscosity coefficient of the wall, respectively, and y is the distance from the wall to the boundary layer edge.

In the outer region for attached boundary layers, the turbulent eddy viscosity is defined by:

$$(\mu_t)_{\text{outer}} = KC_{cp}\rho F_{\text{wake}} F_{\text{kleb}}(y) , \quad (23)$$

where K and C_{cp} are constant equal to 0.0168 and 1.6 and $F_{\text{Kleb}}(y)$ is Klebanoff intermittence factor:

$$F_{\text{kleb}} = \left[1 + 5.5\left(\frac{C_{\text{kleb}} y}{y_{\max}}\right)^6\right]^{-1} , \quad (24)$$

and:

$$F_{\text{wake}} = \min . \begin{cases} y_{\max} F_{\max} \\ C_{wk}\, y_{\max}\, u_{\text{Diff}}^2 / F_{\max} . \end{cases} \quad (25)$$

C_{kleb} is Klebanoff constant equal to 0.3, C_{wk} is a constant equal to 0.25 and:

$$u_{\text{Diff}} = (\sqrt{u^2 + v^2 + w^2})_{\max} - (\sqrt{u^2 + v^2 + w^2})_{\min} . \quad (26)$$

$F_{\max}$ and $y_{\max}$ are determined from the following function:

$$F(y) = y|\Omega|[1 - \exp(-y^+/A^+)] , \quad (27)$$

such that the peak value of $F(y)$ between the wall and the boundary layer edge is defined as $F_{\max}$ and the value of y at this point is $y_{\max}$.

TURBULENCE MODIFICATION

A problem with Baldwin-Lomax model is encountered when it is applied in treating flow about slender bodies at incidence [12]. In the separated flow region, it becomes difficult to determine the correct value of $F_{\max}$, which is necessary for evaluating $\mu_{t,\text{outer}}$. In attached flow, there is only one maximum for $F(y)$ in the radial direction and $F_{\max}$ is simply found. When separated flow occurs, two maxima for $F(y)$ are encountered. The first peak occurs in the boundary layer and a second layer peak exists due to the presence of vortex sheet. If Baldwin-Lomax model is used to obtain $F_{\max}$, the second maximum in $F(y)$ is obtained. This provides values of $\mu_{t,\text{outer}}$ that are much too high, resulting in distortion or a washout of the features in the computed flow [15]. A modification to Baldwin-Lomax model has been proposed by Degani and Schiff and applied by Sturek et al. [3]. For each axial station, a maximum value of the scaling length, $y_{\max}$, is defined as 1.8 times the value of $y_{\max}$ on the windward ray. A peak in $F(y)$ is defined, if the value of $F(y)$ drops below 90% of the local maximum. Where two separate, distinct peaks in $F(y)$ exist, the peak closer to the body is chosen. If the two peaks in $F(y)$ merge into one abnormally large peak (or a peak cannot be found at all), the value of $F_{\max}$ is frozen at the value used for the previous roll angle.

NUMERICAL SOLUTION PROCEDURE

Equation 1 is discretized in hexahedrons using the cell centered finite volume technique (Figure 1). Since the conservative variables are assumed to be defined by their cell averages, the volume integral over a cell is expressed by:

$$\int_v \frac{\partial \underline{U}}{\partial t} dV + \int_s (\bar{\bar{H}}.n) dS = 0 \,, \tag{28}$$

and for steady flow reduces to:

$$\int_S (\bar{\bar{H}}.n) dS = \sum_{m=1}^{6} \bar{\bar{H}}_{pm} . \int_{S_{pm}} n dS = 0 \,, \tag{29}$$

where $\bar{\bar{H}}_{pm} = \frac{1}{2}(\bar{\bar{H}}_p + \bar{\bar{H}}_m)$.

In this equation, p represents the central cell and m is the number of neighboring cells. If it is assumed that the tensor $\bar{\bar{H}}$ remains constant across each face of the cell and that cell face area vectors are oriented in the positive coordinate directions, Equation 29 may be written as:

$$\begin{aligned} &\bar{\bar{H}}^{n+1}_{k,l} . dS^{n+1}_{k,l} + \bar{\bar{H}}^{n+1/2}_{k+1/2,l} . dS^{n+1/2}_{k+1/2,l} \\ &\quad + \bar{\bar{H}}^{n+1/2}_{k,l+1/2} . dS^{n+1/2}_{k,l+1/2} - \bar{\bar{H}}^{n}_{k,l} . dS^{n}_{k,l} \\ &\quad - \bar{\bar{H}}^{n+1/2}_{k-1/2,l} . dS^{n+1/2}_{k-1/2,l} - \bar{\bar{H}}^{n+1/2}_{k,l-1/2} . dS^{n+1/2}_{k,l-1/2} \\ &\quad = 0 \,, \end{aligned} \tag{30}$$

where n, k and l represent streamwise, tangential and radial directions, respectively, and dS is the cell face area vector in the relative direction. With conservative variables given at the first cell face (n), all terms of the flux tensor are available in cell P (Figure 1), except for the gradients of the velocity components and temperature as well as div.u. The gradient in cell P is defined by the following definition of the conservative variables as cell averages [16]:

$$\text{grad } \phi_p = \int_{V_p} \text{grad } \phi \, dV / \int_{V_p} dV \,, \tag{31}$$

where $\phi = u, v, w$, or T.

Using the gradient theorem, the integral in Equation 31 can be expressed by a surface integral, which is approximated as:

$$\begin{aligned} \text{grad } \phi_p &= \int_{V_p} \phi \underline{n} dS / \int_{V_p} dV \\ &= \sum_{m=1}^{6} \phi_{pm} \int_{S_{pm}} \underline{n} \, ds / \int_{V_p} dV \,, \end{aligned} \tag{32}$$

where,

$$\phi_{pm} = \frac{1}{2}(\phi_p + \phi_m) \,.$$

The discretization of viscous terms in these flow equations, which is derived by Muller and Rizzi [16] (based on the above relation), is not suitable for this computation because it introduces false shear stress in the free stream, consequently, producing large error in calculation of eddy-viscosity, especially in the calculation of $F_{\max}$. Since this approach is grid dependent, especially for calculating the turbulent eddy viscosity coefficient, it is better to change the average of properties by difference to:

$$\text{grad } \phi_p = \sum_{m=1}^{6} (\phi_p - \phi_m) \frac{1}{2} \Big[\int_{S_p} \underline{n} dS + \int_{S_m} \underline{n} dS \Big] / \int_{V_p} dV.$$

In the space marching procedure, it is necessary to prevent the departure solution that is inherent in the physics of the boundary layer. This is conducted through using Vigneron technique with the following substitutions:

$$(E)^n_{k,l} = E^*(dS^n_{k,l}, U^n_{k,l}) + E^p(dS^n_{k,l}, U^{n-1}_{k,l}) \,, \tag{33}$$

where the form of E^* and E^P are given by Equation 17 and $dS^n_{k,l}$ and $U^n_{k,l}$ indicate the location where the geometry and the physical variables are evaluated, respectively.

To extract the required flow properties from the flux vector E^*, it is better to change the dependent

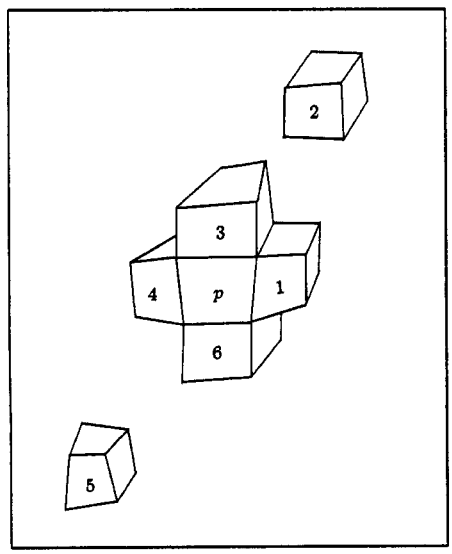

Figure 1. Basic hexahedron p and neighboring cells 1 to 6 (2 and 5 are set apart).

variable from E^* to the vector of conserved variable U through the following linearization:

$$E^* = A^{*n-1}U^n \ , \tag{34}$$

where,

$$A^{*n-1} = \frac{\partial E(dS^n, U^{n-1})}{\partial U^{n-1}} \ . \tag{35}$$

The discretized conservation law Equation 30, then takes the following form:

$$\begin{aligned} A^{*n}_{k,l}\delta^{n+1}U_{k,l} = &-(A^{*n}_{k,l} - A^{*n-1}_{k,l})U^n_{k,l} \\ &- [(\bar{\bar{H}}.dS)^{n+1/2}_{k+1/2,l} - (\bar{\bar{H}}.dS)^{n+1/2}_{k-1/2,l}] \\ &- [(\bar{\bar{H}}.dS)^{n+1/2}_{k,l+1/2} - (\bar{\bar{H}}.dS)^{n+1/2}_{k,l-1/2}] \\ &- [E^p(dS^{n+1}_{k,l}, U^n_{k,l}) - E^p(dS^n_{k,l}, U^{n-1}_{k,l})] \ , \end{aligned} \tag{36}$$

where $\delta^{n+1}U = U^{n+1} - U^n$.

The algorithm developed in this study is based on Lawrence application of Roe scheme which is suitable for space marching calculations [7,8,17].

In this scheme, the inviscid portions of the numerical fluxes are defined according to solutions of what will be referred to as steady approximate Riemann problems (StAR problems). The fluxes $\bar{\bar{H}}_{k+1/2,l}$ and $\bar{\bar{H}}_{k,l+1/2}$ are determined separately by splitting them into two one-dimensional StAR problems as follows:

$$\frac{\partial E^*}{\partial x} + D_{m+1/2}\frac{\partial E^*}{\partial k} = 0 \ . \tag{37}$$

The initial conditions are:

$$E^*(k) = \begin{cases} E^*(dS^n_{m+1/2}, U_m) & \text{where} \quad k < k_{m+1/2} \\ E^*(dS^n_{m+1/2}, U_{m+1}) & \text{where} \quad k > k_{m+1/2} \end{cases} \tag{38}$$

where the index m signifies the direction k or l. The coefficient matrix $D_{m+1/2}$ is defined by:

$$D_{m+1/2} = \left(\frac{\partial \bar{\bar{H}}}{\partial E^*}\right)_{m+1/2} .dS_{m+1/2} \ . \tag{39}$$

The solution to the above approximate Riemann problem consists of four constant property regions separated by three surfaces of discontinuity coming from the cell edge and having slopes given by the eigenvalues of $D_{m+1/2}$. The first order accurate inviscid flux consists of a central differencing component plus a first order upwind dissipation term and is given by:

$$\begin{aligned} \bar{\bar{H}}_{m+1/2} = &\frac{1}{2}(\bar{\bar{H}}_m + \bar{\bar{H}}_{m+1}) \\ &- \frac{1}{2}(\mathrm{Sgn}D)_{m+1/2}[\Delta\bar{\bar{H}}_i.dS_{m+1/2}] \ , \end{aligned} \tag{40}$$

where $\Delta\bar{\bar{H}}_i = \bar{\bar{H}}_{m+1} - \bar{\bar{H}}_m$.

In this equation, the matrix, Sgn D is defined as:

$$\mathrm{Sgn}D = R(\mathrm{Sgn}\Lambda)R^{-1} \ , \tag{41}$$

where R is the matrix of right eigenvector and R^{-1}, which is the inverse of the right eigenvector, is the matrix of left eigenvector and SgnΛ is the diagonal matrix which has the following elements:

$$\mathrm{Sgn}\Lambda = \frac{\lambda^i}{|\lambda^i|} \ . \tag{42}$$

The eigenvalues are defined as:

$$\lambda_{1,2,3} = V/u \ , \tag{43}$$

λ_4 and λ_5 are the roots of the following second degree polynomial:

$$a_1\lambda^2_{4,5} + a_2\lambda_{4,5} + a_3 = 0 \ , \tag{44}$$

where,

$$\begin{aligned} a_1 &= (\gamma(1-\omega)+\omega)u^2 - \omega c^2 \ , \\ a_2 &= \omega[\eta_x c^2 - Vu(1-\gamma)] + \eta_x c^2 - Vu(\gamma - 1) \ , \\ a_3 &= V^2 - c^2(\eta^2_x + \eta^2_y + \eta^2_z) \ , \end{aligned} \tag{45}$$

and:

$$V = (dS_{m+1/2}.\underline{u})/dS^n \ , \eta_{x,y,z} = \left(\frac{dS_{m+1/2}}{dS^n}\right)_{x,y,z} .$$

c is the local speed of sound. The left eigenvector is derived from the following equation:

$$R^{-1}(C - \lambda\underline{I}) = 0 \ . \tag{46}$$

where:

$$C = \frac{\partial \bar{\bar{H}}_{m+1/2}}{\partial E^*} \ .$$

The right eigenvector is the inverse of the left eigenvector.

In order to help Roe's Riemann solver to avoid expansion shocks, only at sonic rarefaction $[\lambda^i(U_m, dS_{m+1/2}) < 0. < \lambda^i(U_{m+1}, dS_{m+1/2})]$, the corresponding positive and negative projections are redefined as [18]:

$$\begin{aligned} {\lambda^i_{m+1/2}}^{\pm} = &{\lambda^i_{m+1/2}}^{\pm} \\ &\pm \frac{[\lambda^i(U_{m+1}, dS_{m+1/2}) - \lambda^i(U_m, dS_{m+1/2})]}{4} . \end{aligned} \tag{47}$$

IMPLICIT ALGORITHM

The first order numerical flux is linearized as follows:

$$(\bar{\bar{H}})^{n+1}_{m+1/2} = (\bar{\bar{H}})^{n}_{m+1/2} + \left[\frac{\partial(\bar{\bar{H}})_{m-1/2}}{\partial U_{m+1}}\right]\delta^{n+1}U_{m+1} + \left[\frac{\partial(\bar{\bar{H}})_{m+1/2}}{\partial U_{m}}\right]\delta^{n+1}U_{m} \ . \quad (48)$$

The Roe averaged Sgn$D$ matrix is assumed locally constant for the evaluation of the numerical flux Jacobians of this equation. The resulting block system of algebraic equations is approximately factored into two block tridiagonal systems in the conventional manner and the algorithm is then written as:

$$\left\{\left[A^{*}_{k,l} + \frac{\partial(\bar{\bar{H}}_{k+1/2,l} - \bar{\bar{H}}_{k-1/2,l})}{\partial U_{k,l}}\right]\delta^{n+1}\bar{U}_{k,l} + \frac{\partial\bar{\bar{H}}_{k+1/2,l}}{\partial U_{k+1,l}}\delta^{n+1}\bar{U}_{k+1,l} - \frac{\partial\bar{\bar{H}}_{k-1/2,l}}{\partial U_{k-1,l}}\delta^{n+1}\bar{U}_{k-1,l}\right\}$$

$$= \text{RHS of Equation 36,}$$

$$\left\{\left[A^{*}_{k,l} + \frac{\partial(\bar{\bar{H}}_{k,l+1/2} - \bar{\bar{H}}_{k,l-1/2})}{\partial U_{k,l}}\right]\delta^{n+1}U_{k,l} + \frac{\partial\bar{\bar{H}}_{k,l+1/2}}{\partial U_{k,l+1}}\delta^{n+1}U_{k,l+1} - \frac{\partial\bar{\bar{H}}_{k,l-1/2}}{\partial U_{k,l-1}}\delta^{n+1}U_{k-1,l}\right\}$$

$$= A^{*}_{k,l}.\delta\bar{U}_{k,l} \ . \quad (49)$$

BOUNDARY CONDITIONS

In general, the initial condition of data plane for the marching method must be supplied from an auxiliary computation. A conical grid is selected and the flow variables are initially set equal to free-stream values. The solution is marched downstream from an initial station and after each step, the new solution is reselected as the initial values. When changes in the total density are very small (e.g. less than 10^{-3}), the variables are constant along rays and conical solution is generated. The solution is then marched along the streamwise direction. For the ogive cylinder computations, the tip of the ogive is replaced with a cone tangent to the ogive at $x = 0.71$ cal.

The no-slip conditions are applied at the wall by allowing no flux through the boundary cell interfaces. Viscous stresses and the wall pressure are extrapolated using zero-gradient extrapolation as follows:

$$\tau_{k,\text{wall}} = \tau_{k,l},$$

$$P_{k,\text{wall}} = P_{k,l}. \quad (50)$$

In this study, the wall is adiabatic, the temperature at the wall is also extrapolated and the wall heat conduction is set to zero.

GRID GENERATION

The primary grids are generated by the simple algebraic method. To set the domain limits approximately, the outer shock is defined by Taylor-MacColl solution and the outer boundary is set at 1.2 times the distance between the shock and body surface. Therefore, there are enough grids at the free stream zone to capture shock. Finally, grid points are clustered along the radial direction according to Roberts stretching function [19]:

$$z = \frac{\beta + 1 - [\beta - 1][\frac{\beta+1}{\beta-1}]^{1-\eta}}{[\frac{\beta+1}{\beta-1}]^{1-\eta} + 1} \ . \quad (51)$$

The positive vectors of the grid points are then given by $r = r_0 + z\ (\mathbf{R} - r_0)$, where r_0 and $\mathbf{R}$ represent the body and the outer boundary radius and β is the stretching parameter. In the circumferential direction, the spacing is constant.

ADAPTIVE GRID

An adaptive grid capability [2] is used in this work for PNS code in order to maintain adequate resolution of the viscous layer. The strategy involves checking for the value of y^+, Equation 22, at the first grid node above the body surface and adjusting the grid stretching parameter to maintain this value of y^+ within the desired range, $5 < y^+ \leq 10$. This check is made only at wind and lee sides of the model. The stretching parameter is varied linearly between the extremes determined at the wind and lee sides for grid nodes at circumferential stations of the pitch plane.

RESULTS

Model Geometry

The dimensions of the ogive cylinder models are shown in Figures 2 and 3. The length of these models is six calibers with a cylinder diameter of one caliber. The grid for these computations consists of 77 points radially, which are stretched between the body and the outer layer and an equal spacing of points circumferentially at increments of 3 degrees. The marching step

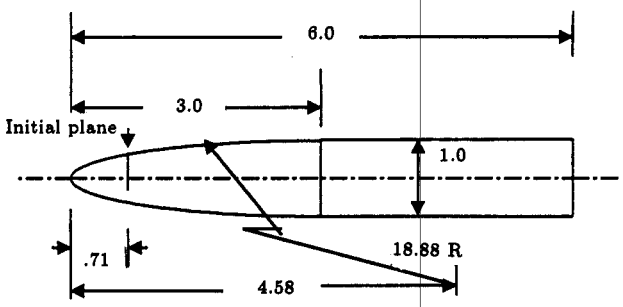

Figure 2. Secant ogive-cylinder model configuration.

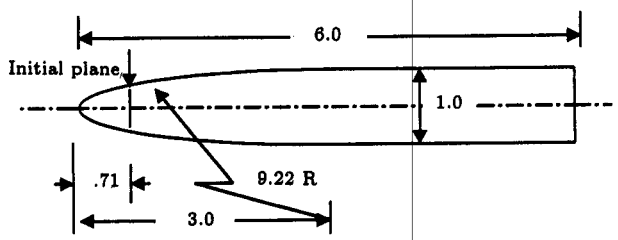

Figure 3. Tangent ogive-cylinder model configuration.

size required at the nose tip is 10^{-4} caliber in order to resolve the boundary layer profile. When the solution is converged, the step size can be enlarged to 10^{-3} caliber and marching will be continued down stream.

Comparison Between Computation and Experiment

The flow field and sectional pressure distribution around SOC and TOC are computed at 10° angle of attack and Mach number of 4. Figure 4 compares computed results with the experimental data [12]. The results indicate a 3-4 percent discrepancy between the two results. The reason for this discrepancy in the attached flow portion might be due to the dissipative nature of the first order upwinding. In addition, in the separated zone, the error will increase further and the separation incipient point will occur later than in the experimental results.

Figures 5 and 6 demonstrate the comparison between pressure distribution at 6° angle of attack and

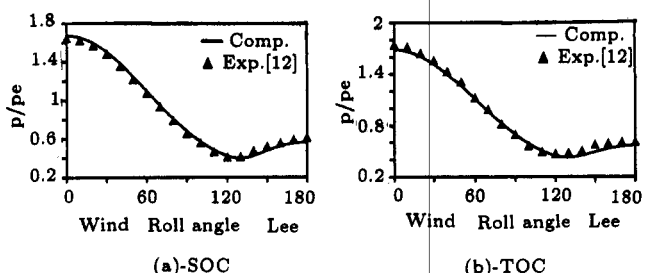

Figure 4. Circumferential surface pressure distribution for SOC and TOC configurations; $M = 4$, $\alpha = 10°$, $Re = 2.13 \times 10^7$ /m, $X/D = 3.13$.

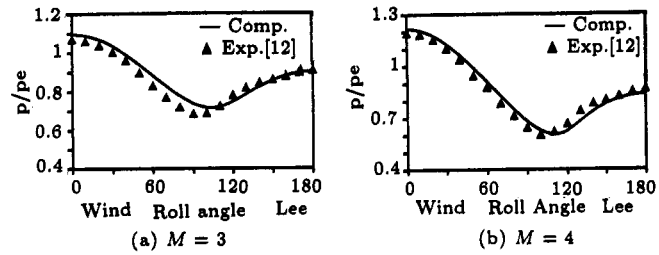

Figure 5. Circumferential surface pressure distribution for SOC configuration; $M = 3$ and 4, $\alpha = 6°$, $Re = 2.13 \times 10^7$ /m, $X/D = 5.77$.

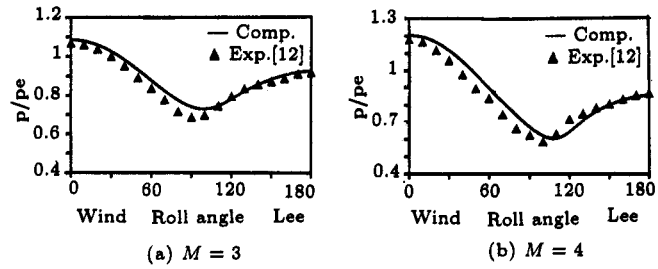

Figure 6. Circumferential surface pressure distribution for TOC configuration; $M = 3$ and 4, $\alpha = 6°$, $Re = 2.13 \times 10^7$ /m, $X/D = 5.77$.

Mach 3 and 4 and the experimental data [12]. The maximum local difference between the experiment and computation are below 10 percent.

As the angle of attack increases, the separation region becomes dominant. At 10° angle of attack and Mach 3, the discrepancies between the present calculated pressure distribution results increase. As is evident from Figures 7 and 8, these differences are about 30-40 percent at 110° roll angle. This is mainly due to the dominance of the separation zone in the flow field. Some reasons for the above differences are:

1. The turbulence model has not correctly captured the physical phenomena.
2. The number of grids employed are not sufficient.
3. In a separated zone, the subsonic region will grow possibly invalidating the application of PNS equations.

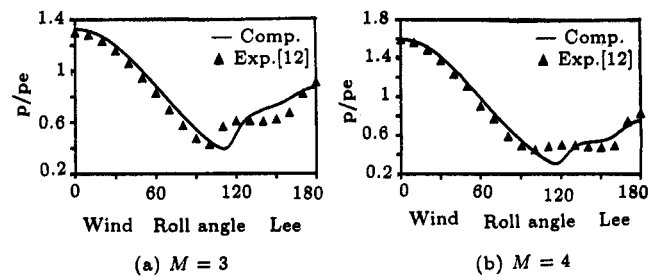

Figure 7. Circumferential surface pressure distribution for SOC configuration; $M = 3$ and 4, $\alpha = 10°$, $Re = 2.13 \times 10^7$ /m, $X/D = 5.77$.

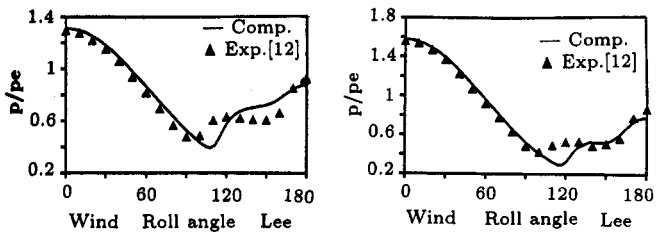

(a) $M = 3$ (b) $M = 4$

Figure 8. Circumferential surface pressure distribution for TOC configuration; $M = 3$ and 4, $\alpha = 10°$, $Re = 2.13 \times 10^7$ /m, $X/D = 5.77$.

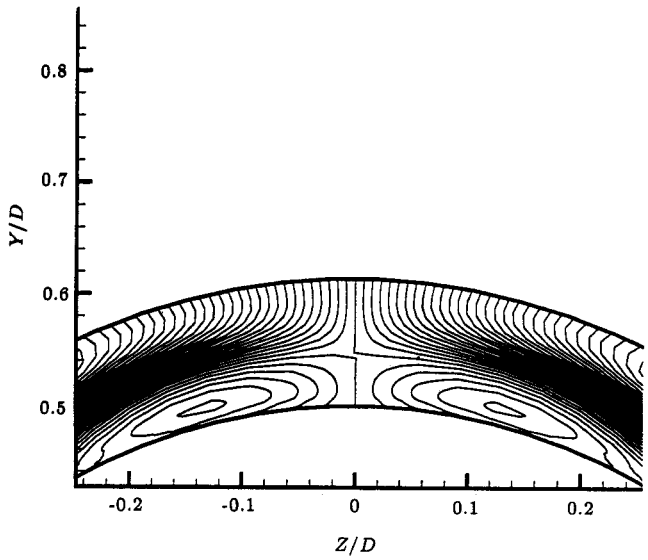

Figure 9. Vortex structure for SOC configuration.

Figure 9 shows a well-defined vortex structure and the secondary flow for Mach 4 at $x = 5.99$. To predict the onset of separation, the grid resolution plays an important role. In this test case, when using coarse grid (i.e., 36 grids circumferentially are used), the separated zone will not be captured, but increasing the grids (120 grids circumferentially) makes the separated region apparent. In addition, the obtained pressure at wind and leeward are in good agreement with the experimental data. The time of computation increases about four times the coarse grid calculation time.

In the present method, the upwinding in the subsonic zone is not eliminated. Actually, in contrast to Lawrence [9], which eliminated upwinding in the subsonic zone, here, the first order upwinding is kept in that zone. The problem with ill conditioning of the eigenvectors did not affect the pressure distribution.

CONCLUSIONS

A 3-dimensional parabolized Navier-Stokes code is developed by using an upwinding scheme throughout the subsonic and supersonic zones. Computational results for the SOC and TOC shell configurations have been generated at attack angle of 6° and 10°. By increasing the angle of attack, the separated zone becomes dominant and the computed pressure distribution would have some discrepancies with experimental results. When the number of grid increases from 36 to 120 circumferentially, the results have better agreement with the experimental data and the separated zone is captured, however, the computation time increases four times with respect to the coarse grid calculation.

NOMENCLATURE

C	speed of sound
C_p	specific heat at constant pressure
dS	cell face area
E_t	total energy
E, F, G	streamwise, tangential and radial flux tensors
F_{Kleb}	Klebanoff intermittence factor
F_{wake}	wake function
$\overline{\overline{H}}_i$	inviscid flux tensor
$\overline{\overline{H}}_v$	viscous flux tensor
$\overline{\overline{I}}$	identity tensor
K	heat conduction coefficient
l	mixing length
L	reference length
M_∞	free stream Mach number
M_ξ	streamwise Mach number
n, k, l	streamwise, tangential and radial directions
$\underline{n}$	normal vector
P	pressure
Pr	Prandtl number
q	heat flux
$\mathbf{R}$	outer boundary radius
R	right eigenvector
Re	Reynolds number
r_0	body radius
S	Sutherland's constant
t	time
T	temperature
$\underline{u}$	velocity vector
u, v, w	velocity components
$\underline{U}$	conservative variables
V_p	cell volume
V_∞	free stream velocity
x, y, z	Cartesian coordinates axes
y^+	distance from wall in law of the wall coordinates

β	stretching factor
γ	constant specific heat ratio
λ	eigenvalues
Λ	diagonal matrix of eigenvalues
μ	viscosity coefficient
μ_t	eddy viscosity coefficient
ρ	density
σ	safety factor
τ	shear stress tensor
ω	streamwise pressure splitting factor
$\sim$	tilde for dimensional quantities
∞	free stream quantities

REFERENCES

1. Schiff, L.B. and Steger, J.L. "Numerical simulation of steady supersonic viscous flow", *AIAA Journal*, **12**(12), pp 1421-1430 (1980).
2. Sturek, W.B. and Schiff, L.B. "Computation of the magnus effect for slender bodies in supersonic flow", *AIAA*, Paper 80-1586 (1980).
3. Sturek, W.B., Weinach, P., Guidos, B.J. and Hodes, B.A. "PNS computations for spinning shell at moderate angle of attack and for long L/D finned projectiles", *AIAA*, Paper 85-0273 (1985).
4. Vigneron, Y.C., Rakich, J.V. and Tannehill, J.C. "Calculation of supersonic viscous flow over delta wings with sharp subsonic leading edges", *AIAA*, Paper 78-1137 (1978).
5. Beam, R. and Warming, R.F. "An implicit factored scheme for the compressible Navier-Stokes equations", *AIAA Journal*, **16**, pp 393-401 (April 1978).
6. Deese, J., Agarwal, R. and Gielda, T. "Computation of supersonic viscous flow about missiles and bodies at high angle of attack using PNS and Navier-Stokes solver", *AIAA*, Paper 89-0527 (1989).
7. Lawrence, S.L., Tannehill, J.C. and Chaussee, D.S. "An upwind algorithm for the parabolized Navier-Stokes equations", *AIAA*, Paper 86-1117 (1986).
8. Lawrence, S.L., Chaussee, D.S. and Tannehill, J.C. "Application of an upwind algorithm to the three-dimensional parabolized Navier-Stokes equations", *AIAA*, Paper 87-1112 (1987).
9. Lawrence, S.L., Chaussee, D.S. and Tannehill, J.C. "Development of a three-dimensional upwind parabolized Navier-Stokes code", *AIAA Journal*, **28**(6), pp 971-972 (June 1990).
10. Harvey, A.D., Acharya, S. and Lawrence, S.L. "Solution adaptive grid procedure for the parabolized Navier-Stokes equations", *AIAA Journal*, **30**(4), pp 953-962 (April 1992).
11. Baldwin, B.S. and Lomax, H. "Thin layer approximation and algebraic model for separated turbulent flows", *AIAA*, Paper 78-257, 16th Aerospace Science Meeting (Jan. 1978).
12. Raklis, R.P. and Sturek, W.B. "Surface pressure measurements on slender bodies at angle of attack at supersonic speeds", U.S. Army Ballistic Research Laboratory, Aberdeen Proving Ground, Maryland ARBRL-MR-02876 (AD A064097) (Nov. 1978).
13. d'Ambrosio, D. and Marsilio, R. "A numerical method for solving the three-dimensional parabolized Navier-Stokes equations", *Computers and Fluids*, **26**(6), pp 587-611 (1997).
14. Tiegang, L., Ruquan, W. and Songhe, S. "An implicit-explicit algorithm for the parabolized Navier-Stokes equations", *ACTA MECHANICA SINICA*, **10**(2), pp 129-135 (May 1994).
15. Gee, K. and Cummings, R.M. and Schiff, L.B. "Turbulence model effects on separated flow about a prolate spheroid", *AIAA Journal*, **30**(3), pp 655-665 (March 1992).
16. Muller, B. and Rizzi, A. "Runge kutta finite volume simulation of laminar transonic flow over the ONERA M6 wing using the Navier-Stokes equations", FFA TN 1987-06 (1987).
17. Roe, P.L. "Approximate Riemann solvers, parameter vectors and difference schemes", *Journal of Computational Physics*, **43** (1981).
18. Chackravarthy, S.R. and Szema, K.Y. "Euler solver for three-dimensional supersonic flows with subsonic packets", *Journal of AIRCRAFT*, **24**(2), pp 73-83 (Feb. 1987).
19. Anderson, D.A., Tannehill, J.C. and Pletcher, R.H. "Computational fluid mechanics and heat transfer", Hemisphere, New York, USA (1984).